

SCIENTIFIC PAPER

Forecasting research of Mixing Uniformity of Cerium Chloride Solution under Microwave heating

Chao Lv^{1,2*}, Yanlong Liu², Zhang Lu Lu²

¹ State Key Laboratory of Complex Nonferrous Metal Resources Clean Utilization, Kunming University of Science and Technology, Kunming 650093, Yunnan, China.

² Key Laboratory of Vibration and Control of Aero-Propulsion System Ministry of Education, Northeastern University at Qinhuangdao, Qinhuangdao 066000, Hebei, China.

<https://doi.org/10.2298/CICEQ240712002L>

Received 12.7.2024.

Revised 27.12.2024.

Accepted 22.1.2025.

* Corresponding author: CHAO LV; e-mail: lvchao@neuq.edu.cn

Abstract: Cerium oxide is an important strategic resource and a key raw material for many functional materials in high-tech fields. Microwave heating is an important method to prepare cerium oxide. In the study of cerium oxide prepared by microwave heating, the variation of the polarity factor inside the solution during heating was explored. In addition to thermal effects, microwave heating also exerts electromagnetic influences that promote the mixing of the solution. This study presents both physical experiments and numerical simulations of the mixing behavior of cerium chloride solutions under microwave exposure. The results reveal that under the influence of the microwave electromagnetic field, the mixing uniformity of the solution remains consistent and stable across the entire region. and the VMD-SSA-LSTM model was proposed to forecast the mixing uniformity under different process conditions. The results show that the mixing effect of cerium chloride solution under microwave is better than that under conventional heating. The selected forecast model saves time and energy and can accurately forecast the above situation. In addition, the forecast effect is best when the modal number k of VMD decomposition is selected as 3.

Key words: Cerium Oxide, Physical Experiment, Numerical Simulation, VMD-SSA-LSTM, Forecast

Highlights

- A simulation model of electromagnetic force inside the tube was established using energy equation
- Microwaves have thermal and electromagnetic mixing effects
- The model can accurately predict the mixing uniformity of solutions under different conditions

INTRODUCTION

Micro-nano cerium oxide is an important rare earth oxide, which has stable chemical properties, excellent thermal stability and good safety. It has been applied in food safety detection, food wastewater treatment and other related fields^[1-3]. Micro-nano cerium oxide is cheap, non-toxic, stable in chemical properties and excellent in oxygen storage and release^[4-5]. As an additive, it can also prolong the service life of some specific coating materials^[6-7]. In addition, it can improve the denitration efficiency of the catalyst and improve the ability of sulfur resistance and water resistance^[8]. Therefore, it also has high research value and wide application in chemical mechanical polishing, fuel cell, medicine^[9] and other fields^[10-12].

In the preparation of cerium oxide, microwave is a high efficiency, non-pollution, non-contact, penetrating and adsorption selectivity of bulk heating method^[13-17].

In microwave preparation of cerium oxide, the mixing uniformity of reactants has a great influence on the conversion of cerium oxide. Increasing the mixing uniformity of cerium chloride solution can make the cerium chloride solution contact with gas phase materials sufficiently, thus achieving the effect of refining droplets^[18-21].

It is time-consuming and laborious to study the mixing effect in the preparation of cerium oxide under different conditions, which often requires a large number of numerical simulations or experiments. How to accurately analyze the mixing of materials in the preparation of cerium oxide and predict the final preparation results through data is particularly important.

In this study, the UDF (User-Defined Function) feature of Fluent was first used to program the formula for the mixing uniformity index. Then, simulations were conducted under different power levels (3 – 5 kW), liquid concentrations (0.02 – 0.1), and time intervals (0.8 s – 2.4 s) to obtain the variation of mixing uniformity over time. The simulation results provided high-dimensional time-series data, which were used as input to the proposed VMD-SSA-LSTM model for predicting mixing uniformity and improving preparation efficiency.

In the current context of the rapid development of artificial intelligence, combining machine learning with practical problems has become an effective way to solve complex problems. In forecasting research, Luan^[22] put forward LSTM forecasting model based on VMD. In this paper, the discharge data of Shalizhai Hydrological Station from 2010 to 2019 are predicted, and the forecasting effect is compared with other models. The results show that VMD-LSTM model can obviously improve the stability of runoff forecasting and reduce the forecasting error; Lu^[23] predicted the sales volume of new energy vehicles by fusing variational modal decomposition (VMD) method and long-term memory neural network (LSTM) model. Firstly, VMD decomposition was used to decompose the data into multiple modal components, and LSTM models were constructed for each component. Finally, more accurate results were obtained by integrating the forecasting status of each component. The research shows that compared with other forecasting models, this method has lower forecasting error and better final effect; Cao^[24] built SSA-LSTM model based on PM 2.5 concentration data in Changsha from May to August, 2023, and made comparative experiments with other models. Experimental results show that the goodness of fit (R²) of SSA-LSTM model is improved by 45.93%, 31.55% and 19.12% compared with single LSTM, PSO-LSTM and WOA-LSTM models, respectively. It can provide certain reference value for formulating PM 2.5 related preventive measures; Liu^[25] proposed a hybrid model of VMD based on rolling time window, improved ISSA and LSTM for forecasting futures price time series. The empirical results show that VMD-ISSA-LSTM model performs best on high-frequency data, which is helpful to

improve the forecasting quality and provide effective support for financial risk control and investment decision-making; Pan^[26] aims to improve the accuracy of short-term power load forecasting model, and combines signal decomposition, ensemble learning, intelligent optimization algorithm and deep learning to build a combined forecasting model. Aiming at the problem of data quality, an improved VMD-SG filter is introduced to smooth and reduce noise. In order to solve the parameter adjustment problem of LSTM, sparrow optimization algorithm is used to optimize the original model. The above literature shows that the combination of signal decomposition, optimization algorithm and deep learning has good applicability and advantages in the prediction of complex dynamic systems.

In terms of mixing uniformity, Li et al. ^[27] proposed to use information entropy to calculate the index weight to evaluate the mixing uniformity of tobacco. Ju et al. ^[28] used a BP neural network to establish a nonlinear relationship between mixing uniformity and weight to predict the uniformity of components. Liu et al. ^[29] proposed an intelligent identification method for concrete uniformity based on dynamic mixing, which solved the problem of insufficient detection methods in the concrete mixing process. In summary, the application of machine learning in complex process control and uniformity evaluation has gradually matured, especially in dynamic multivariate data analysis and resource saving, which provides a reference for this study.

In the process of microwave mixing and preparation of cerium oxide products, the mixing state of materials and the concentration distribution of products have strong timeliness, so the machine learning algorithm of LSTM is suitable for predicting the above states; And for different time periods, different power conditions and liquid concentration conditions, its specific state presents different change amplitude and trend, which requires VMD decomposition to provide conditions for individual forecasting of each signal. At the same time, the optimization of LSTM forecasting by SSA can greatly improve the reliability of the results and improve the accuracy of the forecasting results.

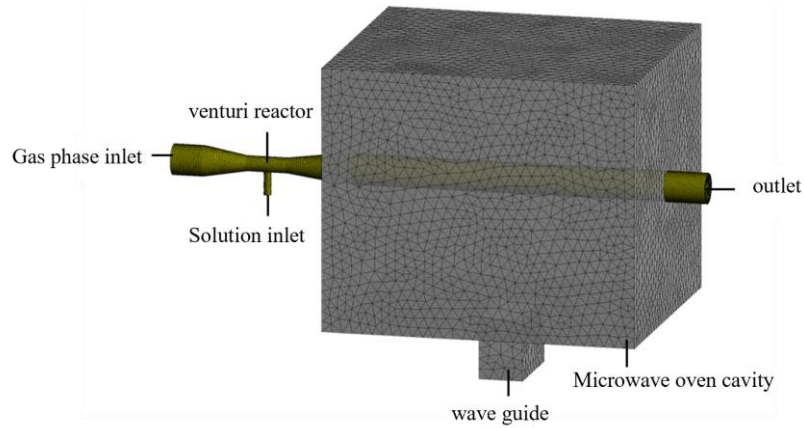
In order to solve the problem of the mixing uniformity of cerium chloride solution, a machine learning optimization scheme based on VMD-SSA-LSTM model is proposed, which provides data-driven through CFD fluid simulation to improve the prediction accuracy. Due to the strong timeliness of the mixing state and concentration distribution in the preparation of cerium oxide, the LSTM model can effectively capture the time series changes, the VMD decomposition further ensures the independent prediction of different signal components, and the SSA algorithm optimizes the prediction accuracy and stability of the LSTM. In this paper, a green and efficient intelligent analysis method is proposed by combining numerical simulation and intelligent prediction algorithms to achieve high-precision prediction of the mixing uniformity of cerium chloride solution under different process conditions.

MATERIALS AND METHODS

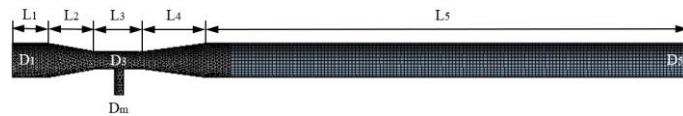
1.1 Model and Mesh

In the HFSS module of Workbench 22R1, the 3D modeling is carried out at a 1:1 scale according to the size of the microwave pyrolysis experimental equipment, and the microwave oven adopts the national standard BJ26 waveguide model. Adaptive meshing is used to solve the solution, and the mesh is refined by the Mesh module. The microwave oven has a three-dimensional tetrahedral grid, and the hot zone and outlet extension have a hexahedral grid. The grid size is 2.5mm, and the total number of grids is 1.4 million. In the Fluent solver module, the microwave oven model is shielded and only the Venturi reactor is mesh refined to improve simulation efficiency and ensure accurate modeling of critical sections. The

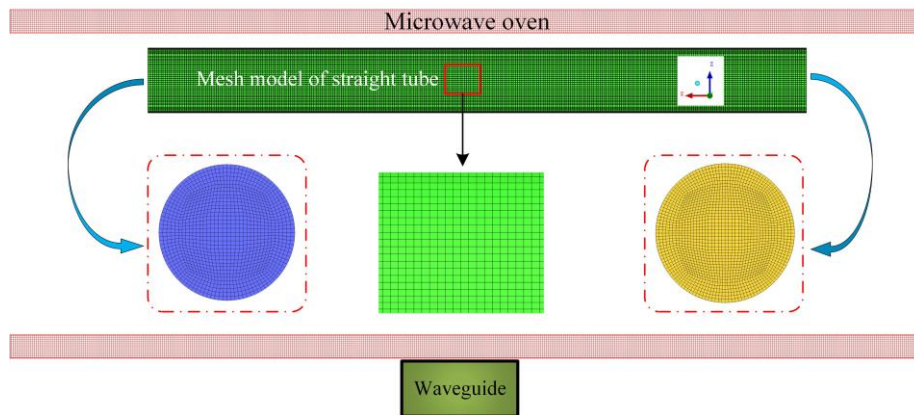
straight pipe part is in the microwave oven, and the mesh adopts a structured meshing method, which is composed of the following steps: 1. a mesh generation method 2, a mesh area division 3, a mesh refinement and adaptive processing 4, a mesh quality and evaluation; Fig. 1a is the overall structure of the venturi pyrolysis reactor, including the inlet and outlet and the waveguide position, Fig. 1b is the structure and meshing of the individual venturi reactor, Fig. 1c is the meshing of the straight pipe of the venturi reactor, the diameter of the pipe is 30mm, the length is 310mm, the coordinates of the left center of the circle are ($X=0, Y=0.135m, Z=0.13m$), and the central axis of the round pipe is ($X=0-0.31m, Y=0.135m, Z=0.130m$). The total number of grids is 700,000, and the minimum orthogonality of the grids is 0.74.



(a) Schematic diagram of pyrolysis plant structure



(b) Schematic diagram of the size and structure of the Venturi reactor



(c) Straight pipe structure and grid

Fig. 1 Geometry and meshing

1.2 Calculation method (VMD-SSA-LSTM method)

1.2.1 Calculation method

Fluent software provides four multiphase flow models: VOF, Mixture, Eulerian-Eulerian and Wet Steam. Because this paper involves droplet diffusion, VOF model is adopted. Phase Couple SIMPLE

algorithm based on pressure-velocity basis and first-order explicit transient algorithm are used in the unsteady calculation. The time step is one thousandth of a second and the iteration times of each time step is 20. This simulation puts forward the following assumptions:

- (1) Fluid is incompressible;
- (2) The single solenoid is 32 W, and the second is 64 W;
- (3) The initial temperature of each area in the flume is 300 K;
- (4) Permeability is constant at 1;

Thermodynamic parameters as well as dielectric properties:

Table 1 Thermodynamic parameters as well as dielectric properties

Sample Material	$C_p(J \cdot kg^{-1} \cdot K^{-1})$	$\lambda(W \cdot m^{-1} \cdot K^{-1})$	$\mu(N \cdot s \cdot m^{-2})$	ϵ_0	ϵ''
CeCl ₃	109.83	600	1.72e-5	72	0.73

Note: λ thermal conductivity、 C_p specific heat capacity、 μ viscosity、 ϵ_0 dielectric constant、 ϵ'' loss factor

The boundary conditions and parameter settings for HFSS are shown in Table 1. For solving flow field and heat transfer problems, it is necessary to define boundary conditions.

Table 1 HFSS boundary conditions

Boundary surface	Boundary condition	Scope
Cavity of microwave oven	Perfect conductor boundary	—
Incentive condition	Excitation of wave port	2.4-2.5 GHz
Scanning step	—	0.01 GHz

In this numerical simulation study, all the boundary conditions are solid wall boundary in static electromagnetic mixing and microwave thermal mixing. Under this condition, the material and product will not be lost. The specific boundary conditions are shown in Table 2.

Table 2 Static boundary conditions

Boundary surface	Boundary condition
Cavity of microwave oven	Ideal conductor
Waveguide	Wave port
Wall surface of reactor	Solid wall

1.2.2 VMD-SSA-LSTM model coupling process

Start by entering the data; Then, the VMD method is used to decompose the original data to obtain k components. SSA was used to optimize the initial parameters of the LSTM, and the search range of the sparrow population size N , the maximum number of iterations M , and the parameter range (number of neurons in the hidden layer H , training times E and learning rate η) were set, and then the mean square error (MSE) was selected as the objective function in the optimization algorithm, and finally the coupling model of the sparrow search algorithm and the long-term and short-term neural network (SSA-LSTM)

was established. The SSA-LSTM prediction model was input into each component separately to obtain k prediction models. Finally, the prediction values of k prediction models are added together.

1.3 Test verification

In order to ensure the reliability of the numerical simulation results in this paper, the verification test as shown in Figure 2(a) is carried out. Start the spotlight (JINBEI) to make the experimental observation position bright enough; Adjust the parameters, placement position and height of the high-speed camera of Thousand-eyed Wolf, so that the image can be clearly displayed on the computer screen responsible for recording; Two electromagnets with a power of 32 W are placed on both sides of the sink to generate electromagnetic fields; The size of the flume is 9.5 cm \times 12 cm. Before the experiment began, distilled water was pre-added to the sink to a height close to 1.5 cm, and the droplets were dripped by the rubber head dropper, which was inserted into the hole at one end of the metal frame and kept fixed.

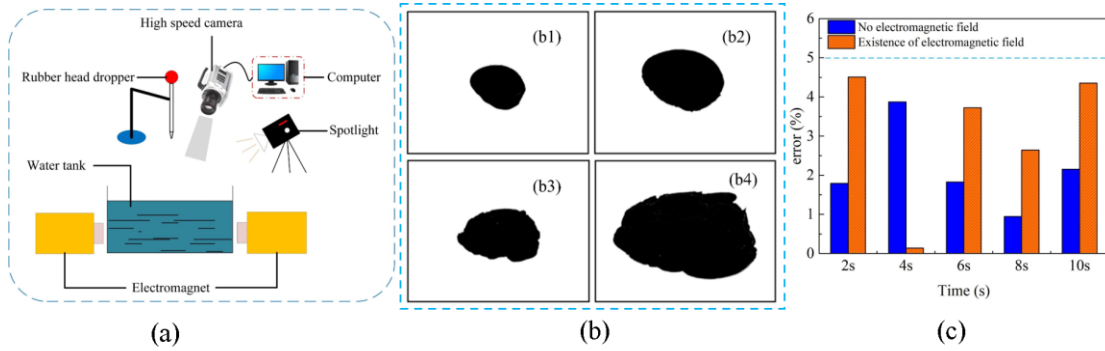


Fig. 2 Verification experiment: (a) Schematic diagram of the validation experiment; (b) Comparison of droplet diffusion areas; (c) Error comparison chart

After all the preparatory work before the test is completed, adjust the rubber head dropper to 1.5 cm height, electrify the electromagnet, drop cerium chloride solution droplets with a particle size of 3.75 mm from the rubber head dropper, and immediately diffuse into the water to form a diffusion area. In order to make the diffusion area more obvious, a little black ink was added as tracer to observe the diffusion of droplets, and the whole process was recorded by high-speed camera.

The diffusion image of cerium chloride solution taken by high-speed camera is grayscale processed and binarized, so that the approximate change of diffusion area in the test can be observed more intuitively, and the processed binarization image is shown in Fig. 2(b), b 1 and b 2 are the diffusion of cerium chloride solution in the ordinary state, and b 3 and b 4 are the diffusion under the action of electromagnetic field. Through comparison, it was found that the diffusion rate of the cerium chloride solution underwent significant changes. In the absence of an electromagnetic field, the diffusion of the cerium chloride solution to the surrounding areas was relatively smooth and regular. However, under the influence of the electromagnetic field, the diffusion of the cerium chloride solution appeared less regular and smooth. The diffusion area under the influence of the electromagnetic field was larger than that without the electromagnetic field, leading to changes in the dynamics and morphology of the diffusion process. Then, the numerical simulation process is carried out. According to the size of the flume, the grid model is established, and the appropriate initialization state and boundary conditions are set. The change of cerium chloride diffusion area within 10 seconds is recorded, and compared with the diffusion area at the same time in the test process, and the error between them is calculated.

The variation of diffusion area of cerium chloride solution with time within 10 s was sorted out. Using Visual Studio software to write C language program to calculate the black area in image processing

technology, import into OpenCV library, and finally present the black area in the drawing, thus obtaining accurate contrast results.

The comparison between numerical simulation results and experimental results is shown in Figure 2 (c).

Through the comparison of numerical simulation and experimental values, it can be seen that the overall error under the action of electromagnetic field is higher than that under the action of no electromagnetic field, and the error has been kept below 5%, which ensures the accuracy of the selected dynamic model, boundary condition setting and numerical simulation model.

1.4 Governing equations

When cerium chloride solution is in electromagnetic field, its motion is affected not only by ordinary hydrodynamic equations, but also by Maxwell equations reflecting electromagnetic law. In this case, if microwave or electromagnetic field interacts with cerium chloride solution, a series of complex physical phenomena and reactions will be caused.

Maxwell's equation is shown in equations 1-4:

$$\nabla \cdot \mathbf{D} = q_e \quad (1)$$

$$\nabla \cdot \mathbf{B} = 0 \quad (2)$$

$$\nabla \times \mathbf{E} = -\frac{\partial \mathbf{B}}{\partial t} \quad (3)$$

$$\nabla \times \mathbf{H} = -\frac{\partial \mathbf{D}}{\partial t} + \mathbf{J} \quad (4)$$

Where B refers to magnetic flux density (Wb/m^2), D refers to electric displacement or flux density (C/m^2), E refers to electric field strength (V/m), H refers to magnetic field strength (A/m), J refers to current density vector (A/m^2), and q_e refers to charge density (C/m^3).

The constitutive equations for the electromagnetic field are determined by Equations 5 and 6, and the magnetic Reynolds number is low during electromagnetic mixing and heating, so magnetic diffusion is ignored.

$$\mathbf{B} = \mu \mathbf{H} \quad (5)$$

$$\mathbf{J} = \sigma(\mathbf{E} + \mu \times \mathbf{B}) \approx \alpha \mathbf{E} \quad (6)$$

where μ is the permeability and σ is the electrical conductivity.

During the electromagnetic mixing of cerium chloride solution, under the influence of microwaves, the charged particles will be subjected to electromagnetic forces, i.e., Lorentz force and electric field force, from which the formulas are derived:

$$\mathbf{F}_l = \mathbf{J} \times \mathbf{B} = \alpha \mathbf{E} \times \mu \mathbf{H} = \alpha \mu \mathbf{E} \times \mathbf{H} \quad (7)$$

$$F_e = qE \quad (8)$$

where q is the amount of charge (C).

In the process of microwave heating, the microwave energy is absorbed by the droplets and converted into heat, which can be expressed by the following formula:

$$Q = \frac{1}{2} \omega \varepsilon_0 \varepsilon'' |E|^2 \quad (9)$$

The equation, ω refers to the angular frequency (rad/s), ε_0 refers to the free space permittivity ($8.85 \times 10^{-12} \text{ F/m}$), ε'' refers to the corresponding loss factor, $|E|^2$ refers to the modulus of the electric field, and Q is the energy absorbed or converted (J).

Choose from standard k - ε models and Euler-Euler multiphase flow models to simulate fluid mixing and flow in the lumen. The Lorentz force [30] and the electric field force are added to the momentum equation as source terms. The theoretical equation is as follows:

Momentum Equation:

$$\frac{\partial(\rho u_i)}{\partial t} + \nabla \cdot (\rho u_i u_j) = -\nabla P + \mu_{\text{eff}} \nabla^2 u_i + \rho g + F_l + F_e \quad (10)$$

P is the pressure (Pa); μ_{eff} is the effective viscosity (Pa·s); g is the acceleration due to gravity ($m \cdot s^{-2}$); F_l is the Lorentz force (N), F_e is the electric field force (N);

Energy Equation:

$$\frac{\partial(\rho T)}{\partial t} + \text{div}(\rho u T) = \text{div}\left(\frac{k}{C_p} \text{grad} T\right) + S_T \quad (11)$$

Among them, C_p is the specific heat capacity; T is the temperature; k is the heat transfer coefficient of the fluid; S_T is the internal heat source of the fluid and the part of the fluid that converts mechanical energy into heat energy due to viscosity, sometimes referred to as the viscous dissipative phase.

When predicting the mixing uniformity under different process conditions, the VMD signal of the data set should be decomposed first, and the decomposition steps are as follows: Equation (12)-(14) is understood after the split of Equation (15).

(1) It is assumed that the input signal $f(t)$ consists of k modal components and k is the center frequency of each eigenmode function $u_k(t)$. Firstly, Hilbert transform is performed, and the decomposed signal of modal function is obtained according to single-side spectrum, as shown in Equation (12). Then, the center frequency $\exp(-j\omega_k t)$ of each decomposed signal is estimated, and the

frequency spectrum of the decomposed signal is converted to the baseband by shifting the frequency, as shown in Equation (13).

$$\left(\delta(t) + \frac{j}{\pi t} \right) * u_k(t) \quad (12)$$

$u_k(t)$: The eigenmode function with finite bandwidth with stricter constraints is redefined.

Defined as:

$$u_k(t) = A_k(t) \cos(\phi_k(t))$$

Where $\delta(t)$ -pulse function.

$$\left[\left(\delta(t) + \frac{j}{\pi t} \right) * u_k(t) \right] \cdot \exp(-j\omega_k t) \quad (13)$$

(2) The square norm of the decomposed signal gradient is calculated to obtain the signal width, as shown in Equation (14). The limiting principle is that the sum of each modal function is equal to the input signal f , so that the sum of the estimated widths of each modal function is minimized. The final constrained variational problem is as follows:

$$\left\| \partial_t \left[\left(\delta(t) + \frac{j}{\pi t} \right) * u_k(t) \right] \cdot \exp(-j\omega_k t) \right\|^2 \quad (14)$$

VMD decomposes the input signal $x(t)$ into k , each corresponding to a specific frequency band. The basic goal is to decompose the input signal into multiple band-restricted signals $u_k(t)$ so that each modality is smoothed across its own frequency band. The optimization problem of VMD can be expressed as:

$$\begin{aligned} \min_{\{u_k\}, \{\omega_k\}} & \left\{ \sum_k k \left\| \partial_t \left[\left(\delta(t) + \frac{j}{\pi t} \right) * u_k(t) \right] \cdot \exp(-j\omega_k t) \right\|^2 \right\} \\ \text{s.t.} & \sum_k k u_k = f \end{aligned} \quad (15)$$

Where: $\{u_k\} = \{u_1, \dots, u_k\}$; $\{\omega_k\} = \{\omega_1, \dots, \omega_k\}$.

(3) In order to transform the constrained variational problem into an unconstrained variational problem, an augmented Lagrangian function is proposed to obtain the optimal solution of the constrained variational problem, as shown in Equation (16).

$$\begin{aligned} L(\{u_k\}, \{\omega_k\}, \lambda) &= \alpha \left\| \sum_k \partial_t \left[\left(\delta(t) + \frac{j}{\pi t} \right) * u_k(t) \right] \cdot \exp(-j\omega_k t) \right\|_2^2 + \\ & \left\| f(t) - \sum_k u_k(t) \right\|_2^2 + \langle \lambda(t), f(t) - \sum_k u_k(t) \rangle \end{aligned} \quad (16)$$

Where: α is the quadratic penalty factor; $\lambda(t)$ is a Lagrangian multiplication operator.

(4) The saddle point of formula (16) is obtained by the alternating direction multiplier method, and the optimal solution of formula (15) is obtained by iterating u_k^{n+1} , ω_k^{n+1} and λ^{n+1} , where u_k^{n+1} is obtained by formula (17).

$$u_k^{n+1} = \arg \min \left\{ \begin{array}{l} \alpha \Sigma_k \left\| \partial_t \left[\left(\delta(t) + \frac{j}{\pi t} \right) * u_k(t) \right] \cdot \exp(-j\omega_k t) \right\|_2^2 + \\ \left\| f(t) - \Sigma_k u_k(t) + \frac{\lambda(t)}{2} \right\|_2^2 \end{array} \right. \quad (17)$$

(5) In order to transform equation (17) above the frequency domain, Fourier isometric transform can be used to obtain quadratic optimization. The result of solving the problem is shown in Equation (18). Similarly, the center frequency iteration problem can be transformed above the frequency domain to obtain the minimum value of ω_k^{n+1} , as shown in equation (19), and ω_k^{n+1} is obtained by equation (20).

$$\bar{u}_k^{n+1}(\omega) = \frac{\bar{f}(\omega) - \sum_{i \neq k} \bar{u}_i(\omega) + \frac{\bar{\lambda}(\omega)}{2}}{1 + 2\alpha(\omega - \omega_k)^2} \quad (18)$$

$$\omega_k^{n+1} = \arg \min \left\{ \int_0^\infty (\omega - \omega_k)^2 |\bar{u}_k(\omega)|^2 d\omega \right\} \quad (19)$$

$$\omega_k^{n+1} = \frac{\int_0^\infty \omega |\bar{u}_k(\omega)|^2 d\omega}{\int_0^\infty |\bar{u}_k(\omega)|^2 d\omega} \quad (20)$$

Where: $\bar{u}_k(\omega)$ is the Wiener filter of $\bar{f}(\omega) - \sum_{i \neq k} \bar{u}_i(\omega)$;

ω_k^{n+1} is the center of the power spectrum of the current modal function.

The mixing degree is an important indicator to represent the mixing capability of electromagnetic mixing and conventional heating mixing for cerium chloride solution. Therefore, the mixing uniformity formula is introduced to quantify the mixing degree of the cerium chloride solution. When M approaches 100%, it indicates a higher mixing degree.

$$M = \left[1 - \left[\frac{\sum_{i=1}^n (X_i - \bar{X})^2}{(n-1)} \right]^{\frac{1}{2}} / \bar{X} \right] \times 100\% \quad (21)$$

When the mixing uniformity reaches approximately 95%, it is considered a state of micromixing, and when it reaches 98%, it is regarded as uniformly mixed.

RESULTS AND DISCUSSION

2.1 Mixing status of cerium chloride solution under microwave irradiation

Microwave mixing ^[31] of cerium chloride solution at time $t=0$ is carried out. Under the conditions of microwave power of 3-5 kW and liquid phase concentration of 0.02-0.1, the concentration distribution of cerium chloride solution within 2.4 s is shown in Figure 3.

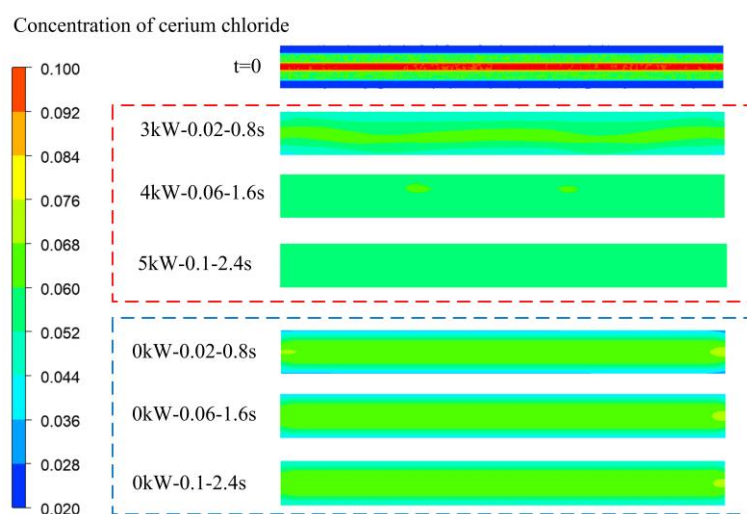


Fig. 3 Concentration distribution of cerium chloride under different process conditions

As shown in Fig. 3, under the reference of free state, microwave shows its influence on the concentration distribution of cerium chloride solution. When the concentration of cerium chloride solution is 0.02 and the time is 0.8 s, the microwave power of 3 kW makes the cerium chloride solution achieve the mixing effect; When the concentration is 0.06 and the time is 1.6 s, the microwave power is increased to 4 kW, and the cerium chloride solution achieves better mixing effect; When the concentration is 0.1 and the time is 2.4 s, the concentration distribution of cerium chloride in the model tends to be consistent and stable under the influence of microwave power of 5 kW, and the cerium chloride solution achieves the best mixing effect.

2.2 Data preprocessing and parameter setting

2.2.1 Data preprocessing

The mixing uniformity data were obtained under the conditions of microwave power 3 kW, 3.5 kW, 4 kW, 4.5 kW, 5 kW, liquid concentration 0.02(100%), 0.04(100%), 0.06(100%), 0.08(100%), 0.1(100%), time $1/5 t$, $2/5 t$, $3/5 t$, $4/5 t$, t and so on.

Firstly, the formula (21) in Section 1.4 was programmed using the UDF (User-Defined Function) feature in Fluent. This allowed the mixing uniformity values at each time step to be output at the end of the respective time step during the calculation process. The values were written to a .txt file, thereby

obtaining the variation of mixing uniformity over time.

The mixing uniformity data is divided into training set and test set, and the ratio of 7: 3 is used as training set, in which the first 70% data are used as training set to train the model; The last 30% of the data is used as a test set, and the validity of the model is verified by predicting the data. The data set distribution is shown in Figure 4.

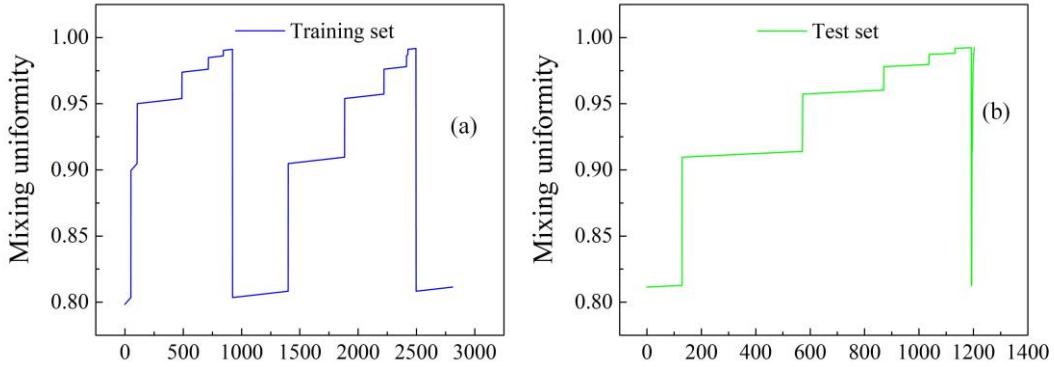


Fig. 4 Data distribution diagram of training set and test set: (a)Training set; (b)Test set

2.2.2 Parameter setting

The parameters of VMD-SSA-LSTM model include input layer and output layer. Adam optimization algorithm is adopted, and the initial learning rate is 0.01, and the learning rate is reduced to one tenth of the original one every 10 iterations. The number of hidden layer units, maximum training period and learning rate are super-parameters of LSTM model, and the ranges are [50, 300], [50, 300] and [0.01, 0.1], respectively. The population size of sparrow is 30, the maximum iteration times are 10, and the decomposition mode numbers are 3, 4 and 5. Producers account for 20%, the safety threshold is 0.8, and RMSE is used as the fitness function.

2.3 VMD decomposition

In this section, the observation method is selected, and the optimal solution is selected according to the data situation, that is, the decomposition situation when the observed modal number k is 3, 4 and 5. VMD decomposition is performed. The maximum decomposition mode number is 5, the moderate bandwidth constraint/ penalty factor is 2500, there is no DC part, and the uniform initialization value of ω is 1. The decomposition result is shown in Fig. 5, and the first behavior is the original data. where X represents the index of the data point

It can be seen that the VMD decomposition method is used to decompose the signals of different frequencies and ranges of the data set, which is beneficial to carry out separate operations on each signal mode and obtain more accurate forecasting results.

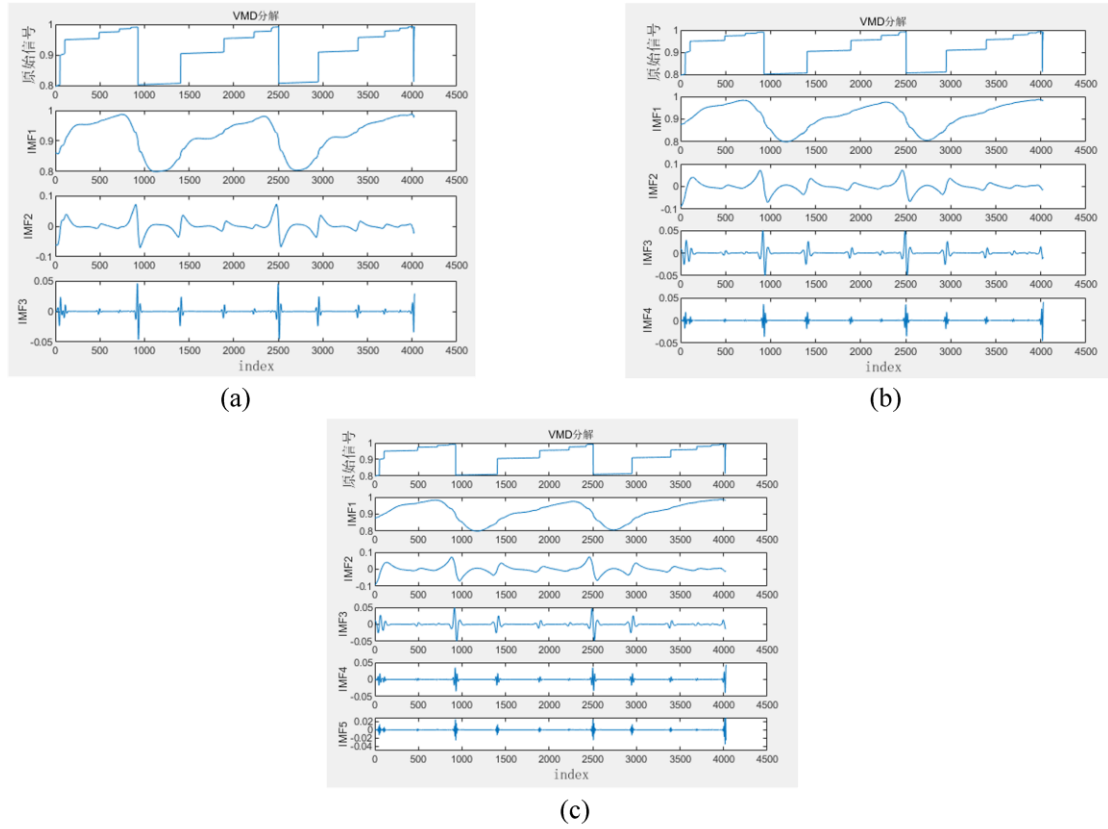


Fig. 5 Modal signal distribution of VMD decomposition: (a) $k=3$; (b) $k=4$; (c) $k=5$

2.4 Forecasting research and result analysis

In the process of wave pyrolysis, there are complex electromagnetic effects on materials, which affect the uniform distribution of materials and materials, and will have an important impact on the pyrolysis results. Therefore, in order to get more accurate forecasting results, this paper uses VMD-SSA-LSTM model to optimize the parameters in the forecasting process to ensure the forecasting accuracy and reliability of the model.

LSTM is optimized by sparrow optimization algorithm to predict each modal signal. Taking the data of the data set as an example, Fig. 6 shows the RMSE curve change of sparrow search algorithm.

As can be seen from Fig. 6(a)、(b)、(c), when $k=3$, 4 and 5, RMSE values tend to be stable from the 5th, 6th and 7th iterations respectively, and their corresponding fitness values are 0.0118, 0.0136 and 0.012 respectively. It can be seen from the figure that the sparrow search algorithm for optimizing LSTM forecasting model is easy to converge.

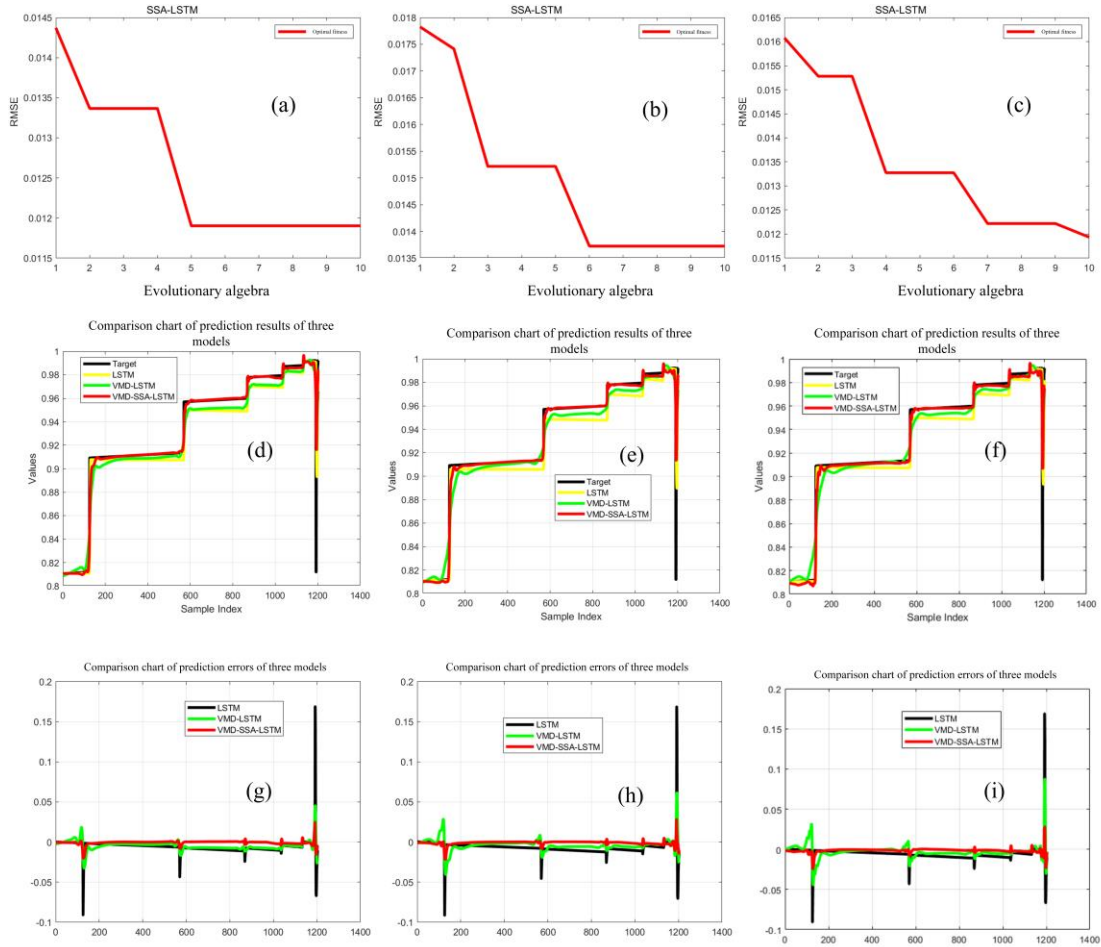


Fig. 6 RMSE curve change and prediction results of sparrow search algorithm: (a) $k=3$; (b) $k=4$; (c) $k=5$; (d) $k=3$; (e) $k=4$; (f) $k=5$; (g) $k=3$; (h) $k=4$; (i) $k=5$

Fig. 6(d)、(e)、(f) shows the comparison chart of the forecasting results of the three models. It can be seen from the chart that during the iteration process, the forecasting value of VMD-SSA-LSTM algorithm is always closest to the real data, and when the real data value fluctuates greatly in the later iteration period, it can alleviate the fluctuation of the value to the greatest extent and maintain the stability of the forecasting data;

As for the forecasting result, the forecasting result of VMD-LSTM algorithm is closer to the real value than that of single LSTM algorithm, which shows the necessity and effectiveness of VMD signal decomposition.

Fig. 6(g)、(h)、(i) shows the comparison diagram of forecasting errors of the three models. It can be seen from the diagram that the forecasting error of VMD-SSA-LSTM algorithm is always lower than that of the other two forecasting models during the iteration process, and when the real data value fluctuates greatly in the later iteration period, the error can fluctuate in a small amplitude near 0 to the greatest extent.

Tables 3 summarize the comparison of forecasting errors between the two models when the modal numbers are 3, 4 and 5. It can be seen from the table that RMSE, MAE and MAPE predicted by VMD-SSA-LSTM algorithm model are obviously lower than those predicted by single LSTM, showing better accuracy.

Table 3 Error comparison of two algorithms

Forecasting algorithm	RMSE	MAE	MAPE(%)
-----------------------	------	-----	---------

$k=3$	LSTM forecasting	0.010429	0.0062302	0.67588
	VMD-SSA-LSTM forecasting	0.0026056	0.0011468	0.12304
$k=4$	LSTM forecasting	0.011174	0.0072928	0.78999
	VMD-SSA-LSTM forecasting	0.0028125	0.0013123	0.14047
$k=5$	LSTM forecasting	0.011272	0.0074544	0.80791
	VMD-SSA-LSTM forecasting	0.0031478	0.0013971	0.14702

It can be seen from Tables 3 that when $k=3$, RMSE decreases by 0.7% and MAE decreases by 0.5%; MAPE decreased by 0.55%; When $k=4$, RMSE and MAE decreased by 0.8% and 0.6% respectively; MAPE decreased by 0.65%; When $k=5$, RMSE and MAE decreased by 0.7% and 0.6% respectively; MAPE decreased by 0.65%.

CONCLUSION

- (1) The experimental results show that microwave can promote the diffusion and mixing of cerium chloride solution, and verify the correctness of the calculation method, kinetic model and calculation results selected by numerical simulation;
- (2) The concentration distribution of cerium chloride solution changed under different microwave technology conditions, and achieved good mixing effect, showing its non-thermal effect;
- (3) Under different modal components (k), the errors of VMD-SSA-LSTM forecasting model are significantly reduced compared with that of single long-short-time memory (LSTM) forecasting. When the VMD component is set to 3, the RMSE of VMD-SSA-LSTM model is the lowest, and the selected decomposition mode number $k=3$.

CONFLICT OF INTEREST

On behalf of all authors, the corresponding author states that there is no conflict of interest. We declare that we do not have any commercial or associative interest that represents a conflict of interest in connection with the work submitted.

REFERENCES

- [1] Chen, C.Y., Lu, J.M., Yao, Q.Z., 2016. Hyperuricemia-related diseases and xanthine oxidoreductase (XOR) inhibitors: An Overview[J]. Chem. Eng. Sci. 22, 2501-2512.
- [2] Xu, Y., Yang, S.H., You, G.X., 2021. Research progress on potential ecological risks and toxic mechanism of nano-ceria[J]. Asian J. Ecotoxicol. 16(01), 43-55.
- [3] Patlán, A., Ayala-García, V., Valenzuela-García, L., et al., 2019. Ywql(endov), exoa and pola act in a novel alternative excision pathway to repair deaminated dna bases in bacillus subtilis[J]. PLoS One. 14 (2), e0211653.
- [4] Min, P., Zhang, S.Z., Xu, Y.H., et al., 2018. Enhanced oxygen storage capacity of CeO₂ with doping-induced unstable crystal structure[J]. Appl. Surf. Sci. 448, 435-443.
- [5] Yoganandan, G., Durgambika, V., Manoj, P., et al., 2022. Nano-sized cerium vanadium oxide as corrosion inhibitor: a microstructural and release study[J]. Electrochim. Acta. 425, 140696.
- [6] Richa, B., Sreeja, N., Krishna, K., et al., 2022. UV resistant wood coating based on zinc oxide and cerium oxide dispersed linseed oil nano-emulsion[J]. Mater. Today Commun. 30, 103177.

- [7] Diksha, D.T., Ananthkumar, M., 2022. Evaluation of cerium oxide nanoparticle coating as corrosion inhibitor for mild steel[J]. *Mater. Today: Proc.* 49, 2007-2012.
- [8] Li, N., Chen, Z.D., Wang, J.J., et al., 2022. Research progress of low temperature NH₃-SCR catalyst based on ceria[J]. *Mater. Rev.* 36(8), 54-63.
- [9] Wang, C.Y., Tong, P., Li, C., et al., 2019. Effect of cerium oxide nanoparticles on radiosensitivity of cisplatin-resistant human lung adenocarcinoma cells[J]. *Carcinog., Teratog. Mutagen.* 31(6), 464-468.
- [10] Zhang, L., Zhu, L.M., Zhou, T.F., et al., 2022. Study on the grinding characteristics of sapphire with the assistant of cerium oxide liquid[J]. *Mater. Des.* 215, 110451.
- [11] Bhusankar, T., Kisoo, Y., Jonghoon, K., et al., 2022. In situ growth of self-composed cerium iron oxide hierarchal structures as a novel anode electrocatalyst for direct methanol fuel cells[J]. *Ceram. Int.* 48, 3628-3635.
- [12] Yang, H., Jia, L., Zhang, Z.P., et al., 2022. Novel cerium-based MOFs photocatalyst for photocarrier collaborative performance under visible light[J]. *J. Catal.* 405, 74-83.
- [13] Galema S. Microwave chemistry[J]. *Chemical Society Reviews*, 1997, 26(3): 233-238.
- [14] Kappe C O. Controlled microwave heating in modern organic synthesis[J]. *Angewandte Chemie International Edition*, 2004, 43(46): 6250-6284.
- [15] Roberts B A, Strauss C R. Toward Rapid, "Green", Predictable Microwave-Assisted Synthesis[J]. *Accounts of Chemical Research*, 2005, 38(8): 653-661.
- [16] Frank, Wiesbrock, Richard, et al. Microwave-Assisted Polymer Synthesis: State-of-the-Art and Future Perspectives[J]. *Macromolecular Rapid Communications*, 2004, 25(20): 1739-1764.
- [17] Gerbec J A, Magana D, Washington A, et al. Microwave-enhanced reaction rates for nanoparticle synthesis[J]. *Journal of the American Chemical Society*, 2005, 127(45): 15791-15800.
- [18] Lv C, Lv X, Zhao Q Y. Simulation and Optimization of Gas-gas Venturi Jet Reactor [J]. *Rare metal*, 2022, 46(03): 394-401.
- [19] Lv C; Zhang T A; Dou Z H; Zhao Q Y; Numerical simulation of preparation of ultrafine cerium oxides using jet-flow pyrolysis, *Chinese Journal of Rare Metals*, 2019, 38(12): 1160-1168.
- [20] Lv C, Yin H X, Liu Y L, et al. Optimization Research on Preparation of CeO₂ Using Microwave Heating Method Based on Regression Orthogonal Design[J]. *JOM*, 2023, 75(7): 2421-2429.
- [21] Lv C, Zhang T A, Dou Z H, et al. Numerical simulation of preparation of ultrafine cerium oxides using jet-flow pyrolysis, *Rare Metals*, 2019, 38(12): 1160-1168.
- [22] Luan C. River discharge forecasting method based on VMD-LSTM [J]. *Water Resources & Hydropower of Northeast China*, 2024, 42(02): 23-29.
- [23] Lu Z P, Yu X J, Lu C Y. Forecasting method of new energy vehicle sales volume based on VMD and LSTM model [J]. *Journal of Wuhan University of Technology (Information & Management Engineering)*, 2023, 45(04): 546-551.
- [24] Cao H J, Li Z Y. Study on Air Quality Forecasting Based on SSA-LSTM Model [J]. *Modern Information Technology*, 2024, 8(04): 142-146+152.
- [25] Liu Y J. Research on Futures Price Forecasting Based on VMD-ISSA-LSTM Model with Rolling Time Window [D]. *Shandong University*, 2024.
- [26] Pan S Y. LSTM Short-term Power Load Forecasting Based on Ensemble Learning and Intelligent Optimization Algorithm [D]. *China University of Mining and Technology*, 2023.
- [27] Li J L, Yin G Y, Zhang G H, et al. Evaluation of Tobacco Mixing Uniformity Based on Chemical Composition[J]. *Proceedings of the 31st chinese control*, 2012, 7552-7555.

- [28] Ju Y P, Li Y G, Hao S W Prediction of mixture mixing uniformity with evolutionary network[J]. Chinese Automation congress (CAC), 2017, 777-781.
- [29] Liu M T, Li B, Yue, S, et al. Intelligent identification of concrete uniformity based on dynamic mixing[J] Signal image and video, 2024, 18(1) 427-436.
- [30] Zhang Y J, Qin W N, Huang X F, A Method for Electromagnetic Force Density Transfer between Shaped Meshes in Coupled Calculation of Magnetic Field and Structural Field[P]. HU BEI: CN104809297A, 2015-07-29.
- [31] Lv C, Liu Y, Li G, et al. Numerical simulation of solution mixing effect and product preparation effect in the process of preparing cerium oxide by microwave heating[J]. Case Studies in Thermal Engineering, 2024, 60.